

Onset of Surface-Tension-Driven Bénard Convection

Michael F. Schatz,* Stephen J. VanHook, William D. McCormick, J. B. Swift, and Harry L. Swinney†
 Center for Nonlinear Dynamics and Department of Physics, The University of Texas at Austin, Austin, Texas 78712
 (Received 5 May 1995)

Experiments with shadowgraph visualization reveal a subcritical transition to a hexagonal convection pattern in thin liquid layers that have a free upper surface and are heated from below. The measured critical Marangoni number (84) and observation of hysteresis (3%) agree with theory. In some experiments, imperfect bifurcation is observed and is attributed to deterministic forcing caused in part by the lateral boundaries in the experiment.

PACS numbers: 47.20.Dr, 47.54.+r, 47.20.Ky, 68.15.+e

The onset of motion in heated fluid layers with a free upper surface has eluded complete understanding ever since Bénard's investigation [1] of these flows established thermal convection as a paradigm for pattern formation in nonequilibrium systems [2]. Rayleigh's analysis [3] of this problem assumed that buoyancy effects, which are always present in layers heated from below, caused convection, but the threshold that Rayleigh predicted did not agree with Bénard's observations. Forty years elapsed before it was recognized that the instability observed in Bénard's studies was not caused by buoyancy but by surface tension gradients [4], as characterized by the Marangoni number M (see Fig. 1). Linear theory [5] yields onset at $M_c = 80$. Weakly nonlinear theory [6,7] predicts a subcritical (hysteretic) transition to a hexagonal pattern. Only a single experimental investigation [8] has systematically examined the onset of convection for layers sufficiently thin such that surface tension forces dominate over buoyancy. That experiment revealed a primary transition to a concentric roll pattern at values of M that decreased as the fluid layers became thinner; for the thinnest layers studied, rolls emerged at M an order of magnitude smaller than M_c from theory.

In this Letter we present evidence for a well-defined primary transition in surface-tension-driven Bénard (Marangoni) convection experiments designed so that surface tension forces dominate over buoyancy to a greater extent than in previous investigations. We observe a hysteretic bifurcation to a defect-free array of hexagonal cells; this bifurcation is modeled by an amplitude equation, which permits comparison to both linear and weakly nonlinear stability theory. We also observe hexagons to arise from an imperfect bifurcation where the hysteresis disappears; this bifurcation is described qualitatively with the addition of a deterministic forcing term to the amplitude equation. In our experiments, surface tension effects are 40 times larger than buoyancy effects, i.e., $M/R \approx 40$, where the Rayleigh number is defined as $R \equiv g\beta \Delta T d^3 / \nu \kappa$ with liquid expansion coefficient β and gravitational acceleration g . A necessary condition for the flow to be surface tension dominated is $M/R \geq 1$ [9]; previous experiments attained $M/R < 11$ [8].

The experiments are performed on a purified silicone oil layer ($d = 0.0419 \pm 0.0005$ cm) that is bounded from below by a 1-cm-thick gold-coated aluminum mirror (Fig. 1) [10]. A uniform air layer ($d_g = 0.0455 \pm 0.0008$ cm) lies between the oil layer and a 1-mm-thick sapphire window. The oil is confined by a Teflon sidewall ring of inner diameter 4.53 ± 0.01 cm. A 50- μm -thick polyethersulfone annular buffer adjacent to the sidewall suppresses convection driven by horizontal temperature gradients [11] that arise from nonuniformities of the contact line at the sidewall. The inner diameter of the buffer determines the radius to height ratio $\Gamma = 45.6 \pm 0.1$ of the convecting region. The oil and the air layer depths each vary by less than 1% over the central 70% of the convecting region, as measured both mechanically and interferometrically. Use of a purified [12] silicone oil (96.7% hexacosamethyldecasiloxane) avoids both condensation [12] and cross-diffusive effects [13] that can affect pattern formation. A temperature gradient is imposed by water cooling the window to a temperature $T_t = 13.320 \pm 0.005$ °C and by computer-controlled heating of the mirror to a temperature T_b that fluctuates less than ± 0.0005 °C. For sufficiently small $T_b - T_t$,

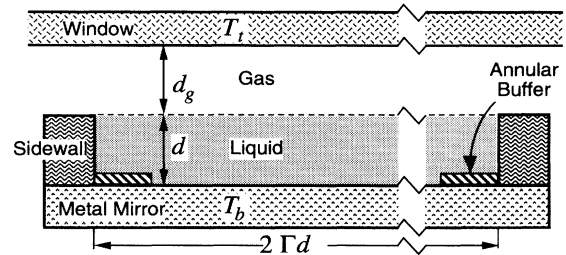


FIG. 1. Cross section of our cylindrical convection cell. The dimensionless control parameter is the Marangoni number $M \equiv \sigma_T \Delta T d / \rho \nu \kappa$, where $\sigma_T \equiv |d\sigma/dT|$ and σ , ρ , ν , and κ are, respectively, the liquid surface tension, density, kinematic viscosity, and thermal diffusivity. The assumption of conductive heat transport is used to obtain the mean temperature across the liquid layer $\Delta T = (T_b - T_t)/(1 + H^{-1})$ with the Biot number $H = k_g d / k d_g$ defined in terms of the thermal conductivities k and k_g of the liquid and gas, respectively.

the surface tension $\sigma(T)$ at the liquid-gas interface is uniform; however, with $T_b - T_t$ sufficiently large, instability causes surface tension variations that drive flow in the bulk. The shadowgraph technique is used to detect onset and to visualize patterns. Images are digitized and background subtracted to improve the signal-to-noise ratio. The time scale in the experiment is set by the vertical diffusion time $t_v = d^2/\kappa = 1.9$ s.

Figure 2 demonstrates that the conductive state undergoes an abrupt transition to hexagons as M is increased slowly ($dM/dt = 10^{-4}$ in units of t_v^{-1}). Just prior to onset, weak circular convection rolls arise near the boundary [upper left and lower right in Fig. 2(a)]; we believe these rolls are driven by static forcing due to the slight mismatch of thermal conductivity between the annular buffer and the liquid. Convection cells first appear within a portion of the boundary rolls after an increase of 2×10^{-3} in $\epsilon \equiv M/M_c - 1$. (M_c is determined from the experiments, as will be described.) Additional hexagons then nucleate from the initial cells and propagate as a traveling front, invading the apparatus until the entire flow domain is filled with the hexagonal pattern [Fig. 2(b)]. The resulting pattern is nearly free from defects, since the lattice is grown from a single "seed crystal" at the boundary. The front propagates across the apparatus in approximately $900t_v$, a time short compared to the horizontal diffusion time $4\Gamma^2t_v \approx 8000t_v$.

Upon decreasing ϵ quasistatically, hexagons persist at parameter values below that for the first appearance of cells (Fig. 3). The transition to the conductive state occurs gradually; the control parameter typically must be decremented through a range of ϵ before the hexagonal convection pattern disappears. The front between hexagonal and conductive states can remain stationary indefinitely (or at least for times long compared to the horizontal diffusion time) for states like Figs. 3(b) or 3(c) if ϵ is held constant.

Near onset, the hexagonal pattern arises from the interaction of three plane wave (roll) solutions, whose wave vectors have a magnitude equal to the critical wave

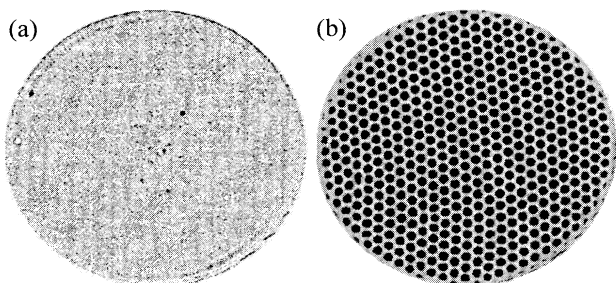


FIG. 2. The abrupt onset of hexagons in Marangoni convection. (a) Just prior to onset, weak convection rolls develop at the boundary for $\epsilon = -5.6 \times 10^{-3}$. (b) A hexagonal pattern fills the entire convection apparatus for $\epsilon = -2.5 \times 10^{-3}$.

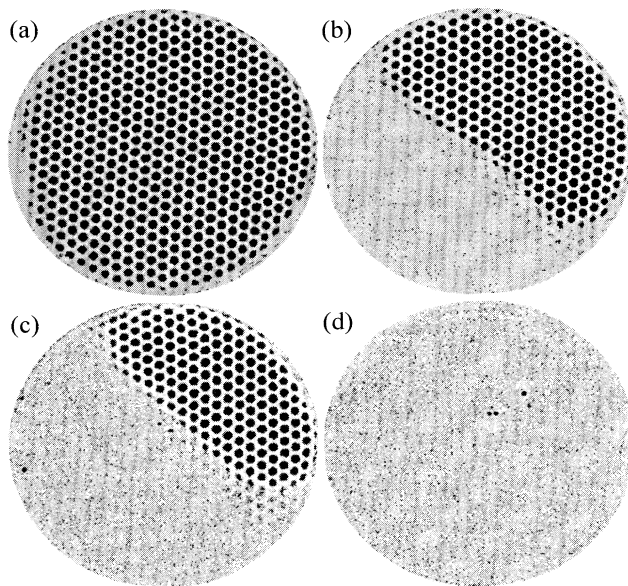


FIG. 3. Return to the conductive state for decreasing ϵ . Below onset hexagonal convection persists at (a) $\epsilon = -2.60 \times 10^{-2}$, (b) $\epsilon = -2.82 \times 10^{-2}$, and (c) $\epsilon = -2.96 \times 10^{-2}$ before disappearing at (d) $\epsilon = -3.20 \times 10^{-2}$.

number and differ in angle by $2\pi/3$ [14]. The evolution of the pattern can then be described by a Landau equation for the amplitude A :

$$\dot{A} = \epsilon A + \alpha A^2 - A^3 + f, \quad (1)$$

with $\alpha > 0$ and f a constant that can account for deterministic forcing. In some cases, the coefficients in Eq. (1) can be computed from the full fluid equations [15]. The existence of hexagons requires $\alpha \neq 0$; thus the bifurcation from the conductive state must be subcritical. The solutions for hexagonal convection and for conduction are both linearly stable over a range of parameters: $\epsilon_\alpha \leq \epsilon \leq 0$ with $\epsilon_\alpha = -\alpha^2/4$ (the conductive state is linearly unstable for $\epsilon > 0$).

Equation (1) is a variational model that exhibits relaxation time dependence governed by a potential function [16], which we first consider for $f = 0$. Over the parameter range, where both conduction and convection are stable, each state corresponds to a minimum of the potential; one state represents the global minimum, while the other state, the metastable phase, represents a local minimum. The potential varies as ϵ changes; at a parameter value ϵ_m (the Maxwell point) both states have equal values of the potential. As ϵ passes through ϵ_m , the states exchange the roles of global stability or metastability. For Eq. (1), the conductive state is globally stable for $\epsilon < \epsilon_m = \frac{8}{9}\epsilon_\alpha$ and metastable for $\epsilon_m < \epsilon < 0$.

To compare the experimental observations to the model, we compute two-dimensional spatial power

spectra from shadowgraph images. The spectra are azimuthally averaged and normalized to the variance of the image intensity. The mean position of the fundamental spectral peak yields the wave number 1.90 ± 0.02 (nondimensionalized by d); linear stability analysis predicts a critical wave number of 1.99 [5]. The wave number is independent of ϵ for the range investigated. The amplitude in Fig. 4 is the square root of the power contained in the spectral peak at the fundamental wave number.

Figure 4 demonstrates that the experimental observations illustrated in Figs. 2 and 3 are consistent with Eq. (1). Hexagonal convection amplitudes for increasing and decreasing ϵ near the bifurcation are fit by a parabola, as suggested by (1) with $f = 0$; from this fit we estimate $M_c = 83.6$ with a precision of ± 0.5 in M . The uncertainty in the accuracy is ± 11 in M , primarily due to the uncertainty in the thermal properties for the silicone oil. From Fig. 4, we also estimate $\epsilon_\alpha = (-3.2 \pm 0.3) \times 10^{-2}$ and $\epsilon_m = (-2.8 \pm 0.3) \times 10^{-2}$ [17]. For increasing ϵ , the convective state shown in Fig. 2(a) is deep within the metastable regime when the initial onset occurs. The weak convection roll at the boundary provides a sufficient perturbation to push the system over the potential barrier, and the front between the two states propagates to spread the globally stable state (hexagons) across the entire apparatus. With decreasing ϵ , hexagonal convection can become metastable; however, the range of parameter values where hexagons are metastable is nearly an order of magnitude smaller than the region of metastability for conduction. This suggests that the transition back to conduction will be more sensitive to small spatial variations in ϵ due to nonuniformities in the depths of both liquid and gas layers. Thus, for values of ϵ near the metastable region of hexagons, the front will move in

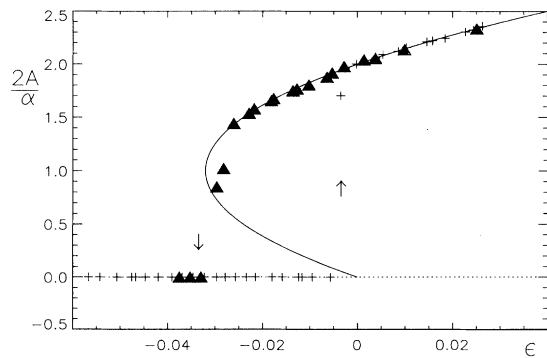


FIG. 4. Hysteresis at the onset of Marangoni convection is demonstrated by a plot of the Fourier mode amplitude A from shadowgraph images vs ϵ . Convection appears suddenly with slowly increasing ϵ (+) and persists below onset for slowly decreasing ϵ (triangles). A fit to the convective branch (—) yields $M_c = 83.6$ ($\Delta T_c = 1.65^\circ\text{C}$), which we use to compute ϵ .

stages to spread the conductive state across the apparatus, as shown in Figs. 3(b) and 3(c).

In some cases, convection appears without hysteresis. This situation arises, for example, in experiments where ϵ is repeatedly increased and decreased, causing conduction and convection to alternate. A reproducible hysteresis is observed for the first cycle after the apparatus is cleaned and assembled (Fig. 4); as the number of cycles increases, hysteresis is observed at smaller values of ϵ and for a smaller range of ϵ . Eventually, the subcritical transition in Fig. 4 evolves to a convective onset that occurs continuously [Fig. 5(a)] after a sufficient number of cycles, which varies from 3 to 15 for different experimental runs. The evolution from a subcritical bifurcation (Fig. 4) to an imperfect subcritical bifurcation [Fig. 5(a)] [18] occurs on a time scale much longer than the horizontal diffusion time. Equation (1) models imperfect bifurcation with $f \neq 0$; for $f > f_c = \alpha^3/27$, hysteresis disappears at the onset of hexagons. In this regime, Eq. (1) qualitatively describes the amplitudes measured from our experiments [Fig. 5(a)]; the difference between the model and the data suggests that a more complex form for f [e.g., $f(\epsilon)$] is necessary for quantitative agreement.

The physical origin of the forcing that causes imperfect bifurcation has not been determined definitively; however, the observation of low amplitude rolls parallel to the lateral boundary [Fig. 5(b)] suggests sidewall boundaries are affecting the flow. Similar structures arise in buoyancy-driven convection with intentional thermal forcing at the sidewall [11], although forcing for surface-tension-driven flow is probably more complex because some deformation of the free surface at the boundary is unavoidably present due to nonuniform contact line pinning at the sidewall. The low amplitude flows become increasingly cellular away from the boundaries and toward the center of the apparatus; moreover, with increasing ϵ above onset, the rolls at the sidewall are supplanted by hexagonal cells as the amplitudes arising from imperfect bifurcation ap-

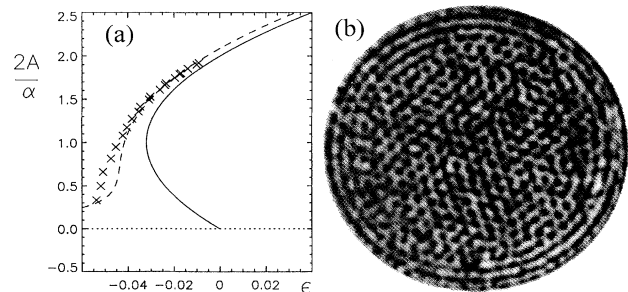


FIG. 5. Imperfect bifurcation in Marangoni convection. (a) Data (\times) are compared to Eq. (1) with $f = 1.3f_c$ (---). The parabola from Fig. 4 (—) is also shown. (b) Shadowgraph image of weak convective flow at $\epsilon = -5.30 \times 10^{-2}$ in the presence of significant deterministic forcing.

proach the amplitudes observed during hysteretic onset [Fig. 5(a)].

Our experimental studies of onset confirm the predictions of theory and suggest an explanation for the puzzling disagreement between previous experiments and theory for the century-old problem of surface-tension-driven Bénard convection. Our determination of $M_c = 84$ is in reasonable agreement with M_c from linear theory [19], and our observation of subcritical bifurcation is in accord with weakly nonlinear theory. Our finding of 3.2% hysteresis sets a standard for comparison to nonlinear theories, whose estimates of hysteresis range from 0.2% [7] to 2.3% [6]. Observation of imperfect bifurcation demonstrates the sensitivity of the primary instability in Marangoni convection to perturbations; the appearance of rolls before hexagons at $M \ll M_c$ in previous experiments [8] may well be due to this sensitivity.

We are grateful to M. Bestehorn, S.H. Davis, R.E. Kelly, and E.L. Koschmieder for helpful discussions. This work is supported by a NASA Microgravity Science and Applications Division Grant No. NAG3-1382. One of us (S.J.V.H.) acknowledges support from the NASA Graduate Student Researchers Fellowship Program.

*Electronic address: schatz@chaos.ph.utexas.edu

†Electronic address: swinney@chaos.ph.utexas.edu

[1] H. Bénard, Rev. Gén. Sci. Pure Appl. **11**, 1261 (1900).

[2] M.C. Cross and P.C. Hohenberg, Rev. Mod. Phys. **65**, 851 (1993).

[3] Lord Rayleigh, Philos. Mag. **32**, 529 (1916).

[4] M.J. Block, Nature (London) **178**, 650 (1956).

[5] J.R.A. Pearson, J. Fluid Mech. **4**, 489 (1958).

[6] J. Scanlon and L. Segal, J. Fluid Mech. **30**, 149 (1967).

[7] A. Cloot and G. Lebon, J. Fluid Mech. **145**, 447 (1984).

[8] E.L. Koschmieder and M.I. Biggerstaff, J. Fluid Mech. **167**, 49 (1986).

[9] S.H. Davis and G.M. Homsy, J. Fluid Mech. **98**, 527 (1980).

[10] Physical properties for the liquid and the gas ($\rho = 0.925 \text{ g/cm}^3$, $\nu = 7.1 \text{ cS}$, $\sigma_T = 0.068 \text{ dyn/cm}^\circ\text{C}$, $k = 1.25 \times 10^4 \text{ erg/cm s}^\circ\text{C}$, $\beta = 1.1 \times 10^{-3} \text{ }^\circ\text{C}^{-1}$, $\kappa = 8.6 \times 10^{-4} \text{ cm}^2/\text{s}$, and $k_g = 2.55 \times 10^3 \text{ erg/cm}^\circ\text{C}$) are obtained from the literature; see, for example, R.R. McGregor, *Silicones and Their Uses* (McGraw-Hill, New York, 1956), and references therein; *CRC Handbook of Chemistry and Physics* (CRC Press, West Palm Beach, 1978), 59th ed.; H.J. Palmer and J.C. Berg, J. Fluid Mech. **47**, 779 (1971).

[11] G. Ahlers, C.W. Meyer, and D.S. Cannell, J. Stat. Phys. **54**, 1121 (1989).

[12] M.F. Schatz and K. Howden, Exp. Fluids (to be published).

[13] E. Moses and V. Steinberg, Phys. Rev. Lett. **57**, 2018 (1986).

[14] S. Ciliberto, P. Coulet, J. Lega, E. Pampaloni, and C. Pérez-García, Phys. Rev. Lett. **65**, 2370 (1990).

[15] S.H. Davis, Annu. Rev. Fluid Mech. **19**, 403 (1987); M. Bestehorn, Phys. Rev. E **48**, 3622 (1993).

[16] B.A. Malomed, A.A. Nepomnyashchy, and M.I. Tribelshy, Phys. Rev. A **42**, 7244 (1990).

[17] ϵ_α is typically an order of magnitude smaller for the onset of hexagons in buoyancy-driven convection; see, for example, E. Bodenschatz, J.R. de Bruyn, G. Ahlers, and D.S. Cannell, Phys. Rev. Lett. **67**, 3078 (1991).

[18] G. Iooss and D.D. Joseph, *Elementary Stability and Bifurcation Theory* (Springer-Verlag, Berlin, 1990).

[19] Linear theory that accounts for the small effects of both buoyancy ($M/R = 39$) and heat transfer ($H = 0.2$; see Fig. 1) predicts $M_c = 86.9$; see D.A. Nield, J. Fluid Mech. **19**, 341 (1964).

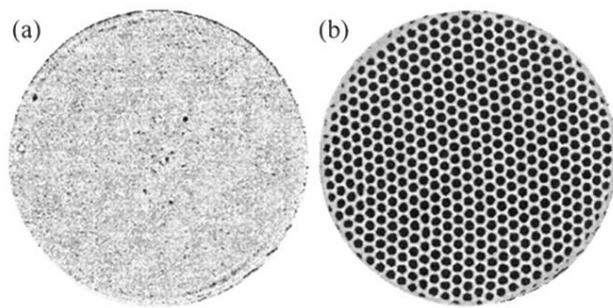


FIG. 2. The abrupt onset of hexagons in Marangoni convection. (a) Just prior to onset, weak convection rolls develop at the boundary for $\epsilon = -5.6 \times 10^{-3}$. (b) A hexagonal pattern fills the entire convection apparatus for $\epsilon = -2.5 \times 10^{-3}$.

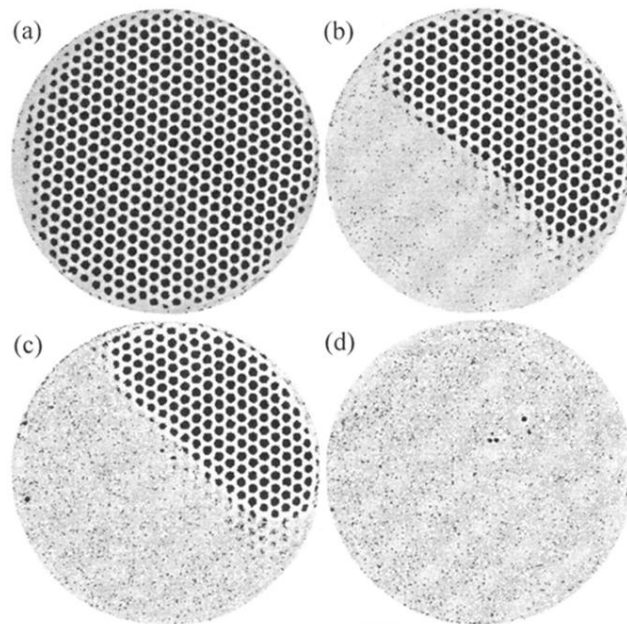


FIG. 3. Return to the conductive state for decreasing ϵ . Below onset hexagonal convection persists at (a) $\epsilon = -2.60 \times 10^{-2}$, (b) $\epsilon = -2.82 \times 10^{-2}$, and (c) $\epsilon = -2.96 \times 10^{-2}$ before disappearing at (d) $\epsilon = -3.20 \times 10^{-2}$.

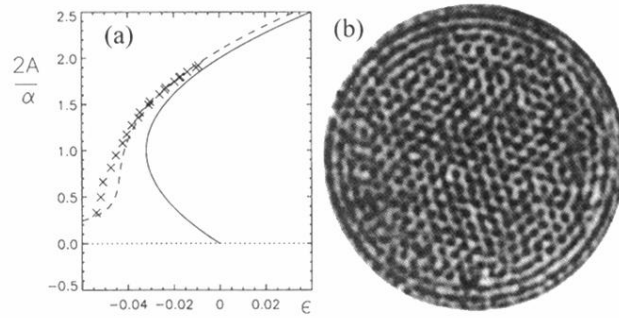


FIG. 5. Imperfect bifurcation in Marangoni convection. (a) Data (\times) are compared to Eq. (1) with $f = 1.3f_c$ (---). The parabola from Fig. 4 (—) is also shown. (b) Shadowgraph image of weak convective flow at $\epsilon = -5.30 \times 10^{-2}$ in the presence of significant deterministic forcing.